ACS APPLIED MATERIALS & INTERFACES

www.acsami.org

Research Article

Back-Surface Passivation of CdTe Solar Cells Using Solution-Processed Oxidized Aluminum

Fadhil K. Alfadhili, Adam B. Phillips,* Kamala Khanal Subedi, Craig L. Perkins, Adam I. Halaoui, Manoj K. Jamarkattel, Bhuiyan M. Anwar, Geethika K. Liyanage, Deng-Bing Li, Corey R. Grice, Yanfa Yan, Randy J. Ellingson, and Michael J. Heben

Cite This: *ACS Appl. Mater. Interfaces* 2020, 12, 51337−51343

Read Online

ACCESS | Metrics & More | Article Recommendations | Supporting Information

ABSTRACT: Although back-surface passivation plays an important role in high-efficiency photovoltaics, it has not yet been definitively demonstrated for CdTe. Here, we present a solution-based process, which achieves passivation and improved electrical performance when very small amounts of oxidized Al^{3+} species are deposited at the back surface of CdTe devices. The open circuit voltage (V_{oc}) is increased and the fill factor (FF) and photoconversion efficiency (PCE) are optimized when the total amount added corresponds to ∼1 monolayer, suggesting that the passivation is surface specific. Addition of further Al^{3+} species, present in a sparse alumina-like layer, causes the FF and PCE to drop as the interface layer becomes blocking to current flow. The optimized deposit increases the average baseline PCE for both Cu-free devices and devices where Cu is present as a dopant. The greatest improvement is found when the Al^{3+} species are deposited prior to the $CdCl_2$ activation step and Cu is employed. In this case, the best-cell efficiency was improved from 12.6 to 14.4%. Time-resolved photoluminescence measurements at the back surface and quantum efficiency measurements performed at the maximum power point indicate that the performance enhancement is due to a reduction in the interface recombination current at the back surface.

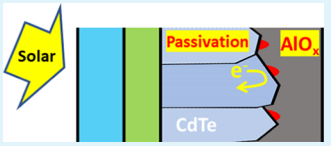

KEYWORDS: *interface passivation, CdTe, back contact, solution processed, alumina*

INTRODUCTION

Recent improvements in the materials and interfaces in CdTe thin-film solar cells have led to increases in the photoconversion efficiency (PCE), with the record now at 22.1%.[1] While the short circuit current density (J_{sc}) is near bandgap-limited values and the fill factor (FF) has increased to 79%,[1] there is still substantial opportunity to increase the open circuit voltage (V_{oc}).[2] As further improvements in the bulk lifetime are obtained through Cl passivation[3] and Se incorporation,[4] and the interface recombination at the front surface is reduced through emitter engineering,[5,6] both critical parameters for device improvement,[7,8] the back interface may soon limit device efficiency.[9] Consequently, research is being focused on developing strategies to reduce back-surface minority carrier recombination while still enabling for efficient majority carrier extraction. Passivated back contacts are also required to enable bifacial operation for higher-energy yields[10] and will be required for future CdTe-based tandems.

A reduction in back-surface recombination can be accomplished by reducing the concentration of electrically active defects at the interface or by creating an electric field to repel minority carriers through electrostatics, doping profiles, or band offsets.[9] Surface passivation in Si has been achieved by several approaches[11] including by depositing alumina by both vacuum and solution processing.[12,13] Alumina has also been explored for passivation of both the rear[14] and front surfaces[15] of $Cu(In,Ga)Se_2$ solar cells. Alumina's potential for passivating CdTe surfaces was demonstrated recently when time-resolved photoluminescence (TRPL) studies reported carrier lifetimes of 27 and 750 ns for CdTe (2 μm thickness)[16] and $Cd_xSe_{1-x}Te$ (2−2.8 μm)[17] layers, respectively, in alumina double heterostructures. The mechanism of the passivation is not yet clear but could be due to a high density of fixed negative charge[18] or the low degree of lattice mismatch (3.7%) between the unit cell of the (0001) surface of Al_2O_3 and the (111) surface of CdTe.[19] These characteristics offer the potential for repelling minority carriers and creating a low defect density interface, respectively.[16,18,20,21]

While demonstration of long carrier lifetimes via an optical measurement is promising, to date there is no clear evidence for back-surface passivation in an operating CdTe device. Previous attempts have included deposition of alumina by atomic layer deposition (ALD)[22] and sputtering.[16] Liang et al. deposited alumina layers in thicknesses up to 5 nm by ALD and tracked the device performance.[22] The baseline PCE of 10.7% was improved to 12.1% when the Al_2O_3 thickness was 1 nm, while thicker deposits led to poorer device performance. A 1 nm layer was reported to be thin enough to allow holes to

Received: July 15, 2020
Accepted: October 22, 2020
Published: November 4, 2020

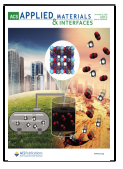

https://dx.doi.org/10.1021/acsami.0c12800
ACS Appl. Mater. Interfaces 2020, 12, 51337−51343

tunnel and thick enough to present a fixed charge to repel minority carrier electrons.[22] However, the data that was presented in the paper was not consistent with this interpretation. First, an improvement in the long-wavelength photoresponse at short circuit was cited as proof of a reduced back-surface recombination rate, but current collection at short circuit when the electric field is the largest is not a good indicator of back-surface passivation. Second, the biggest factor leading to improved PCE (Figure 2a in ref 22) was a flattening of the slope of the $J-V$ curve through zero bias. This increase in the shunt resistance is more consistent with pin-hole blocking. Also, there was no evidence for current blocking when the Al_2O_3 layers were thicker. In contrast, Kephart et al. applied Al_2O_3 by sputtering and saw pronounced kinks in the $J-V$ characteristic at layer thicknesses of 3 and 5 nm. In this case, however, the device efficiency was not improved with the addition of Al_2O_3.[16] Thus, there has been no conclusive evidence to date for enhancement of PV performance in CdTe due to back-surface passivation. Other efforts to passivate the back surface of CdTe have included the use of TiO_2 and NiO,[23,24] but, similarly, the results were not definitive.

Here, we present a solution-based process that reduces back-surface recombination in CdTe solar cells and increases the PCE. Following a process developed for passivating silicon solar cells by deposition of alumina,[25] we employed aluminum acetylacetonate ($Al(acac)_3$) dissolved in methoxyethanol and a spin-coating/heating procedure in an effort to deposit alumina on the back surface of CdTe solar cells. Data from current–voltage ($J-V$) curve analysis, time-resolved photoluminescence, external quantum efficiency (EQE) measurements made at the maximum power point, and Auger electron and X-ray photoelectron spectroscopies provide conclusive evidence that the device improvement is indeed due to back-surface passivation. The optimized process increased the average baseline efficiency for Cu-free devices from 10.4 to 11.7%, while the average PCE for devices made with Cu-doping improved from 12.0 to 12.9%. Application of the $CdCl_2$ activation process after exposure to $Al(acac)_3$ with Cu-doping causes the baseline to be improved from 12.0 to 13.8%.

EXPERIMENTAL CONDITIONS

CdTe device stacks were obtained from the center part of a 60 cm × 120 cm plate produced in a commercial deposition reactor by Willard and Kelsey Solar Group. The large area deposition process produced uniform films, so the initial structure, ~100 nm of CdS and ~3 μm of CdTe on TEC-15M coated soda-lime glass, can be considered to be constant for each experiment. The samples were activated by applying a saturated solution of $CdCl_2$ in methanol and heating to 390 °C in dry air for 30 min. Excess $CdCl_2$ was removed by rinsing with methanol. The aluminum acetylacetonate $Al(acac)_3$ (Sigma-Aldrich Co. LLC, 99.999%) precursor solution was prepared by dissolving 400 mg of as-received powder in 20 mL of 2-methoxyethanol. Two hundred and fifty microliters of the solution was pipetted onto a stationary sample, which was then spun at 2000 rpm for 25 s.[25] Samples were then heated in laboratory air to 300 °C for 10 min. The spinning/heating cycle was performed 1, 3, 5, 7, and 9 times to produce increasingly thicker passivation layers. Devices were formed by depositing 40 nm of Au by thermal evaporation to form a back-metal electrode. Some samples also had a thin layer (3 nm) of Cu deposited by evaporation prior to Au deposition to enhance doping and lower the back contact barrier. In these cases, a subsequent heating step at 150 °C was performed in air to promote Cu diffusion for times ranging between 40 and 80 min. Individual solar cells were precisely defined by laser scribing (0.06 cm^2). Performance statistics were evaluated for relatively large data sets (n > 20). Additional experimental details regarding Auger electron and X-ray photoelectron spectroscopies, $J-V$ and EQE characterization, and photoluminescence are presented below and in the Supporting Information.

RESULTS AND DISCUSSION

Figure 1 shows the $J-V$ curves and performance parameters as a function of the number of spin-coating/heating cycles for

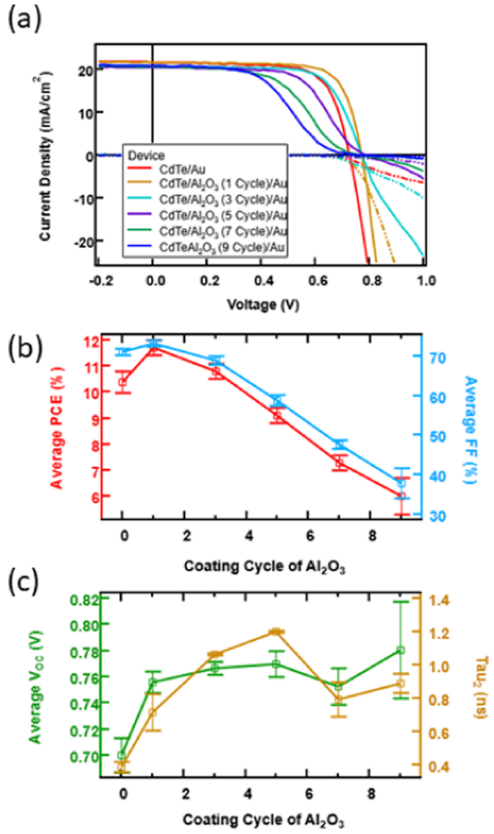

Figure 1. (a) Current density–voltage ($J-V$) curves for the CdTe device with varying number of spin/heat cycles for the Al_2O_3 process. (b) Average power conversion efficiency (PCE) and fill factor (FF) and (c) average open circuit voltage (V_{OC}) and the long lifetime component of the time-resolved photoluminescence (TRPL; τ_2) measurement of the devices as a function of a number of cycles.

samples that had no copper added. Note that the standard deviation in the measured PV parameters for sets of 20 devices in each experiment showed a typical variation of only 1–2% in J_{sc}, V_{OC}, and FF and ~3% in PCE (Table 1). Figure 1a shows the $J-V$ curves for the best devices with zero, 1, 3, 5, 7, and 9 spin-coating/heating cycles. The short circuit current density (J_{sc}) values are essentially constant within error, and a small difference can be attributed to small deviations in the CdS emitter layer thickness. On the other hand, Figure 1c shows that the V_{OC} increases abruptly with the first cycle and stays nearly constant with additional cycles. We also note that it is surprising that the V_{OC} is already fairly high at 700 mV for zero cycles, and this may be due to Cu impurities in the CdTe source materials. The first cycle $J-V$ curve also shows an improved FF but increasing the number of cycles produces first a kink and then a strong blocking effect. Figure 1b shows that the overall efficiency trend is dominated by the FF, with a peak in PCE after the initial increase in the V_{OC}. Data for the full

https://dx.doi.org/10.1021/acsami.0c12800
ACS Appl. Mater. Interfaces 2020, 12, 51337–51343

Table 1. $J-V$ Performance Data for Devices Fabricated With and Without Cu and Al_2O_3 Deposition/Heating Cycles[a]

device		V_{OC} (V)	J_{SC} (mA/cm^2)	FF (%)	PCE (%)
		Without Cu			
CdTe/Au	average	0.700 ± 0.013	21.0 ± 0.2	70.9 ± 0.8	10.4 ± 0.4
	best	0.726	21.5	72.0	11.3
CdTe/Al_2O_3(1 cycle)/Au	average	0.756 ± 0.008	21.2 ± 0.3	73.1 ± 0.9	11.7 ± 0.3
	best	0.770	21.6	74.9	12.5
CdTe/Al_2O_3(3 cycles)/Au	average	0.767 ± 0.005	20.5 ± 0.2	68.9 ± 1.1	10.8 ± 0.3
	best	0.771	20.7	70.4	11.3
CdTe/Al_2O_3(5 cycles)/Au	average	0.755 ± 0.010	20.5 ± 0.2	58.8 ± 1.4	9.1 ± 0.3
	best	0.785	20.4	60.4	9.7
CdTe/Al_2O_3(7 cycles)/Au	average	0.753 ± 0.014	20.4 ± 0.1	47.7 ± 1.2	7.3 ± 0.3
	best	0.772	20.6	50.1	7.9
CdTe/Al_2O_3(9 cycles)/Au	average	0.781 ± 0.037	20.3 ± 0.4	37.9 ± 3.7	6.0 ± 0.7
	best	0.830	20.7	40.1	6.9
		With Cu			
CdTe/Cu/Au 150 °C 40 min	average	0.783 ± 0.004	21.1 ± 0.3	72.5 ± 0.9	12.0 ± 0.2
	best	0.790	21.8	71.5	12.3
CdTe/Al_2O_3(1 cycle)/Cu/Au 150 °C 40 min	average	0.800 ± 0.008	20.8 ± 0.5	76.4 ± 0.8	12.7 ± 0.2
	best	0.806	21.8	75.6	13.3
CdTe/Al_2O_3(1 cycle)/Cu/Au 150 °C 60 min	average	0.818 ± 0.007	20.7 ± 0.4	76.2 ± 0.7	12.9 ± 0.3
	best	0.830	21.5	76.2	13.6
CdTe/Al_2O_3(1 cycle)/Cu/Au 150 °C 80 min	average	0.821 ± 0.006	20.5 ± 0.3	75.8 ± 1	12.7 ± 0.3
	best	0.829	20.7	76.4	13.1

[a]Data is presented for the best device (in terms of PCE) and the population of devices in each data set (n > 20).

population of devices with $Al(AcAc)_3$ processing after $CdCl_2$ activation can be found in Table 1.

Figure 1c shows the carrier lifetimes, which were extracted from biexponential fits to the PL transients. The carrier lifetime, which is associated with the longer-lived component in the PL (τ_2, see the Supporting Information), followed the V_{OC} trend with spin/heating cycles. The PL was excited and detected through the back of the CdTe absorber. With a $1/e$ penetration depth of ~125 nm for the 532 nm light, the measurement should be sensitive to recombination at the back surface. Since no Cu was used in these experiments, possible redistribution of dopants and possible changes at the front interface can be discounted.[26] Control experiments in which devices were exposed to spin/heating cycles without $Al(acac)_3$ showed different V_{OC} behavior that is more consistent with previously reported effects associated with back-surface oxidation in air.[27] Thus, the increase in PL lifetime and the increase in V_{OC} can both be attributed to passivation effects, perhaps due to a reduction in the defect state surface density at the interface or a reduction in rear-surface band bending.[9,10]

Figure 2a–c shows scanning electron microscopy (SEM) images of the CdTe surfaces directly after $CdCl_2$ processing and after the addition of 1 and 5 spin-casting/heating cycles, respectively. Prior to deposition (Figure 2a), the image is characteristic of the polycrystalline films with a grain size of ~300 nm to 1 μm. The images are only subtly changed after 1 spin-casting/heating cycle (Figure 2b) and the grains appear to be smoothed with some edges appearing to be eroded or perhaps decorated with a thin deposit. There is no evidence of a conformal or complete coating. After five cycles, the surface morphology is significantly changed (Figure 2c) and small protrusions, or nodules, are evident. These are ~100 to 200 nm in extent and present on the surfaces of the grains. In some locations, it appears that the grains have developed new terraces (Figure S3), suggesting that the surface energy may have been reduced due to reconstruction. AES mapping

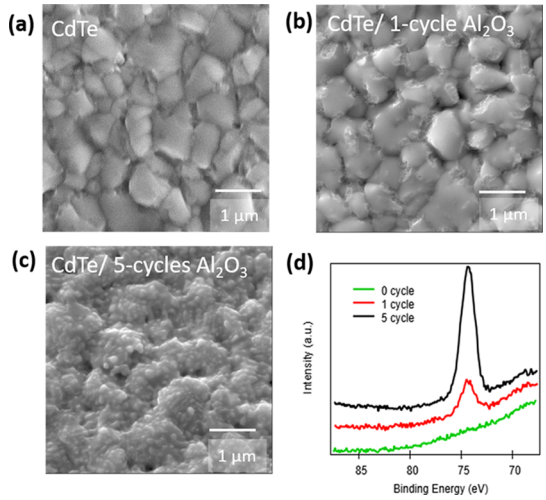

Figure 2. Scanning electron microscope images of CdTe surface (a) without and with (b) one or (c) five cycles of Al_2O_3 processing. (d) Al 2p XPS data without (green), with one (red) and five (black) cycles.

yielded very poor signal-to-noise aluminum maps with no clear correlation between the Al content and the structures observed in the SEM images (see Figure S2). However, aluminum was clearly detected in AES data that was acquired when the Al signal was integrated while scanning 2 μm × 2 μm areas of both the 1-cycle and 5-cycle samples with higher Al signal strength for the latter sample. Interestingly, not even the nodules observed in the SEM images of the 5-cycle sample were well correlated with the aluminum AES signals (see Table S2).

Figure 2d shows Al 2p XPS data collected for zero, 1, and 5 spin/heat cycles. The aluminum signal is evident after only 1 spin/heating cycle and becomes more intense after five cycles. In an attempt to quantify the amount of Al on the surface, an

https://dx.doi.org/10.1021/acsami.0c12800
ACS Appl. Mater. Interfaces 2020, 12, 51337–51343

alumina film prepared by ALD on a CdTe single crystal was examined as a calibration standard. The calibration standard was prepared on the CdTe native oxide using eight water/trimethylaluminum reaction cycles, resulting in an estimated thickness of 1.0 ± 0.5 nm.[28] The Al/(Cd + Te) signal ratio determined by XPS for the sample with 1 spin-casting/heating cycle was approximately 1/10th of that measured for the calibration standard, suggesting that the amount of Al may be considered to be present in a thickness on the order of 1 monolayer. This result, coupled with the nonuniformities observed by SEM and atomic force microscopy (see Figure S5), indicates that the passivation effect is realized through surface chemistry reactions at specific locations on the grains of the polycrystalline film. This suggests the possibility of facet-specific passivation.

Maruyama and Arai produced stoichiometric Al_2O_3 films on silicon wafers by heating $Al(acac)_3$ powder to 150 °C and introducing the entrained vapor to samples heated to temperatures between 250 and 600 °C.[29] The films were adherent, suggesting that the reaction occurred at the surface rather than in the gas phase. Our work suggests that the aluminum deposition reaction from $Al(acac)_3$ is also surface specific in the presence of polycrystalline CdTe. However, at present, due to the rough topography of the surface and the very small amounts of the material involved, we have no direct evidence for the formation of Al_2O_3. Based on the alignment of the spectra by setting the Te^{2-} peak to 572.4 eV,[28] the 74.3 eV binding energy for the peak rules out several possibilities including Al^0 and aluminum halides. Instead, the Al signal is consistent with Al^{3+} bonding found for several alumina oxides.[28] X-ray diffraction and infrared (IR) spectroscopy analyses were inconclusive in identifying surface Al_2O_3, even for samples made with 9 spin/heating cycles. However, when precursor layers approximately 1 μm thick were prepared on soda-lime glass by blade coating and subsequently heated, infrared spectroscopy showed absorption features representative of Al_2O_3 in the range of 1000−500 cm^{-1} (Figure S4).[29]

In an effort to increase the PCE further, we used Cu to increase the level of p-type doping. While Cu has also been employed to reduce the height of the Schottky barrier at the back surface, the lack of roll-over in the 1-cycle Cu-free data suggested that the barrier was already low.[30] Figure 3a shows the $J-V$ curves for a CdTe device with a Cu/Au back contact (3 nm evaporated Cu followed by 150 °C for 40 min in air) as compared to devices fabricated with first surface Al_2O_3 (1 cycle) and then 3 nm of Cu and 40 nm Au with Cu diffusion times (150 °C in air) of 40, 60, and 80 min. After the Cu diffusion process alone (no Al_2O_3), the PCE improved from 10.4 to 12.0% (compare Figures 1a, 3a and see Table 1). Note that the performance of the devices with the optimized standard Cu/Au back contact exceeded the PCE of the devices with one Al_2O_3 cycle and no Cu (12.0 versus 11.7%, respectively). However, introducing the 3 nm of Cu on top of the 1-cycle Al_2O_3 film and employing a 40 min heating increased the best-cell PCE by a full percentage point. Extending the heating time further to 60 min increased the V_{OC} and the FF further without changing J_{SC}, leading to an increase of the PCE of the devices to 12.9% and a best-cell efficiency of 13.6% (Figure 3a and Table 1).

Recent device simulations that explored the use of back buffer layers for high-efficiency CdTe solar cells make it clear that a combined increase in FF and V_{OC} is one hallmark of a reduction in back-surface recombination.[9] On the contrary, J_{SC} is not expected to be increased, nor should the slope of the $J-V$ curve at zero-bias change, as was observed by Liang et al.[22] To further probe whether back-surface passivation is indeed responsible for the improvements observed here, we performed external quantum efficiency (EQE) measurements with the devices biased at their respective maximum power points (MPPs) under an AM1.5 light bias. It is most instructive to examine the wavelength-dependent carrier collection efficiency under this condition, as opposed to typical EQE measurements, which are done at zero-bias (short circuit) conditions without light bias, because the energy bands in the emitter and absorber semiconductor layers will be fairly flat and poised under their normal operating condition. At MPP, it is possible to examine back-surface passivation effects by measuring the collection efficiency for carriers that are generated deeper in the device.

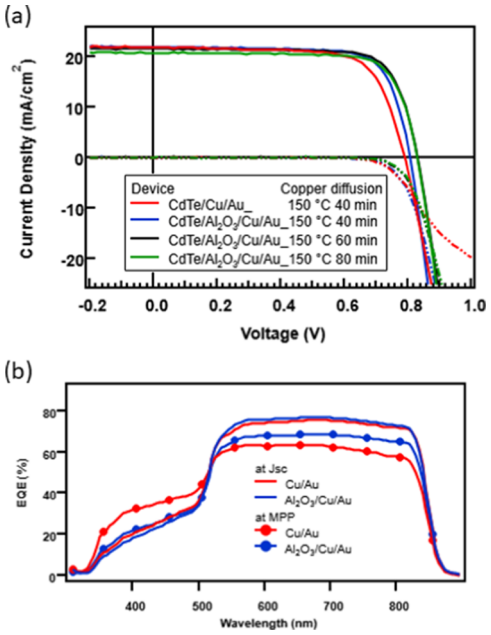

Figure 3. (a) $J-V$ curves of CdTe devices with a standard Cu/Au back contact and one cycle of Al_2O_3 processing with Cu/Au annealed for varying times. (b) External quantum efficiency measurements for the CdTe device with standard Cu/Au back contact and one cycle of Al_2O_3/Cu/Au back contact at short circuit and maximum power point bias.

Figure 3b compares the data obtained at zero bias and at MPP for a device with a standard Cu/Au back contact to that obtained from a device with a 1-cycle Al_2O_3/Cu/Au back contact. We first note that the zero-bias data for the two devices overlaps completely, consistent with the J_{SC} values being the same. This result is expected since the electric field in the absorber is high at zero bias and the impact of back-surface recombination should not be strongly reflected in the data.

Turning to the EQE data at the MPP, the Cu/Au contact (MPP = 650 mV) shows a higher response in the short wavelength region of the spectrum (<500 nm), presumably due to Cu compensation of donor sites in the CdS window layer.[31] The absence of an increase in the short wavelength response for the 1-cycle Al_2O_3/Cu/Au (MPP—675 mV) is consistent with the thin Al_2O_3 layer reducing Cu diffusion into the CdS. In the long wavelength portion of the spectrum (>500 nm), the Cu/Au contact shows a reduction in the carrier collection efficiency. This is due to the downward band

https://dx.doi.org/10.1021/acsami.0c12800
ACS Appl. Mater. Interfaces 2020, 12, 51337−51343

Table 2. $J-V$ Performance Data for Devices Fabricated With and Without 1 Cycle of Al_2O_3 Deposition and Then Subjected to $CdCl_2$ Activation with No Other Thermal Treatment[a]

device		V_{OC} (V)	J_{SC} (mA/cm^2)	FF (%)	PCE (%)
CdTe/$CdCl_2$/Cu/Au	average	0.784 ± 0.006	21.7 ± 0.2	70.6 ± 1.5	12.0 ± 0.3
	best	0.777	21.9	73.8	12.6
CdTe/Al_2O_3 (1 cycle) /$CdCl_2$/Cu/Au	average	0.818 ± 0.007	22.1 ± 0.1	76.4 ± 1.5	13.8 ± 0.4
	best	0.818	23.2	75.7	14.4

[a]Devices were finished with the standard Cu/Au back contact. Data is presented for the best device (in terms of PCE) and the population of devices in each data set (n > 20).

bending at the back surface, which causes minority carrier electrons that are generated nearby to be attracted to the back surface where they will more efficiently recombine.

In contrast, the 1-cycle Al_2O_3/Cu/Au sample shows a long wavelength response that has the same spectral dependence (i.e., slope) as does the zero-bias data. The reduction in the EQE that is constant with a wavelength in comparison to the zero-bias data is a reflection of the fact that the Shockley–Read–Hall contribution to the overall recombination is larger throughout the device when the bands are flatter, as is the case at MPP. However, the fact that the spectral dependence of the EQE is the same as in the zero-bias data, where the internal field is much larger, indicates that the carriers generated throughout the device, regardless of depth, have a similar probability of being collected. Consequently, we can conclude that back-surface recombination has been reduced.

A final set of experiments demonstrated that the process could be considerably simplified. In this case, the $Al(acac)_3$ solution was first pipetted and spun onto the as-grown CdTe device stack and then the $CdCl_2$ treatment was performed. The only high-temperature treatment was used for the standard $CdCl_2$ process (387 °C for 30 min, in air). After the $CdCl_2$ treatment, the Cu/Au back contact was formed as described above (with heating in air for 40 min for both samples). Table 2 shows the measured $J-V$ parameters for these $CdCl_2$/Cu/Au and $Al(AcAc)_2$/$CdCl_2$/Cu/Au devices. Note that these device stacks came from a different production run, which introduced slight differences in performance from the previous data sets. The device results were similar to those found for the single spin/heat cycle, but the performance was improved to higher values. The average V_{OC} for the sample set increased from 0.784 ± 0.006 to 0.817 ± 0.007 mV, while the FF increased from 70.6 ± 1.5 to 76.4 ± 1.1 and the average PCE increased from 12.0 ± 0.3 to 13.8 ± 0.4%. Figure 4a shows the $J-V$ curves for the best-performing devices of each type, while Figure 4b shows the SEM of the CdTe surface after the $Al(acac)_3$/$CdCl_2$ processing. In this data set, there was a statistically significant increase in short circuit current, which could be due to differences in the degree of Cu compensation.

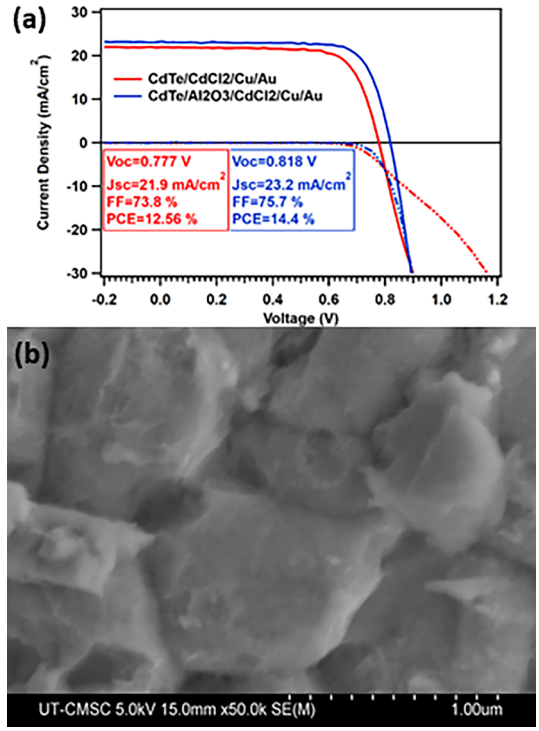

Figure 4. (a) $J-V$ curves for CdTe devices with an evaporated Cu/Au back contact and a device prepared with $Al(acac)_3$ prior to $CdCl_2$ treatment. (b) Scanning electron microscopy image of the CdTe surface for the $Al(acac)_3$/$CdCl_2$ sample.

CONCLUSIONS

We developed a solution-based process that deposits very small amounts of oxidized aluminum (Al^{3+}) species onto the back surface of CdTe device stacks to produce increased V_{OC}, FF, and PCE in finished devices. The binding mechanisms for the Al^{3+} species appear to be site specific and the device performance was optimized when the amount deposited corresponded to ∼1 monolayer. Time-resolved photoluminescence spectroscopy on the back surface and quantum efficiency measurements performed at the maximum power point support the conclusion that interface recombination at the back surface was reduced by back-surface passivation. The mechanism is unclear at the present time, but the results could be due to either the reduction of band bending or the elimination of surface states. Further work in our laboratory will be directed toward discriminating between these two possibilities, understanding the surface chemistry in more detail, and applying the new approach to higher-efficiency devices.

ASSOCIATED CONTENT

Supporting Information

The Supporting Information is available free of charge at https://pubs.acs.org/doi/10.1021/acsami.0c12800.

Experimental details; PL and TRPL data; AES maps and elemental analysis; FTIR, AFM, and additional EQE data (PDF)

AUTHOR INFORMATION

Corresponding Author

Adam B. Phillips – *Wright Center for Photovoltaics Innovation and Commercialization, Department of Physics and Astronomy, University of Toledo, Toledo, Ohio 43606, United States;*

https://dx.doi.org/10.1021/acsami.0c12800
ACS Appl. Mater. Interfaces 2020, 12, 51337–51343

orcid.org/0000-0002-2675-5052; Email: adam.phillips@utoledo.edu

Authors

Fadhil K. Alfadhili − *Wright Center for Photovoltaics Innovation and Commercialization, Department of Physics and Astronomy, University of Toledo, Toledo, Ohio 43606, United States*

Kamala Khanal Subedi − *Wright Center for Photovoltaics Innovation and Commercialization, Department of Physics and Astronomy, University of Toledo, Toledo, Ohio 43606, United States*

Craig L. Perkins − *National Renewable Energy Laboratory, Golden, Colorado 80401, United States;* orcid.org/0000-0002-9036-8698

Adam I. Halaoui − *Wright Center for Photovoltaics Innovation and Commercialization, Department of Physics and Astronomy, University of Toledo, Toledo, Ohio 43606, United States;* orcid.org/0000-0003-0812-6153

Manoj K. Jamarkattel − *Wright Center for Photovoltaics Innovation and Commercialization, Department of Physics and Astronomy, University of Toledo, Toledo, Ohio 43606, United States*

Bhuiyan M. Anwar − *Wright Center for Photovoltaics Innovation and Commercialization, Department of Physics and Astronomy, University of Toledo, Toledo, Ohio 43606, United States*

Geethika K. Liyanage − *Wright Center for Photovoltaics Innovation and Commercialization, Department of Physics and Astronomy, University of Toledo, Toledo, Ohio 43606, United States;* orcid.org/0000-0003-4000-0729

Deng-Bing Li − *Wright Center for Photovoltaics Innovation and Commercialization, Department of Physics and Astronomy, University of Toledo, Toledo, Ohio 43606, United States;* orcid.org/0000-0003-4555-4894

Corey R. Grice − *Wright Center for Photovoltaics Innovation and Commercialization, Department of Physics and Astronomy, University of Toledo, Toledo, Ohio 43606, United States*

Yanfa Yan − *Wright Center for Photovoltaics Innovation and Commercialization, Department of Physics and Astronomy, University of Toledo, Toledo, Ohio 43606, United States;* orcid.org/0000-0003-3977-5789

Randy J. Ellingson − *Wright Center for Photovoltaics Innovation and Commercialization, Department of Physics and Astronomy, University of Toledo, Toledo, Ohio 43606, United States;* orcid.org/0000-0001-9520-6586

Michael J. Heben − *Wright Center for Photovoltaics Innovation and Commercialization, Department of Physics and Astronomy, University of Toledo, Toledo, Ohio 43606, United States;* orcid.org/0000-0002-3788-3471

Complete contact information is available at: https://pubs.acs.org/10.1021/acsami.0c12800

Notes

The authors declare no competing financial interest.

■ ACKNOWLEDGMENTS

This material is based on research sponsored by Air Force Research Laboratory under agreement FA9453-18-2-0037 and FA9453-19-C-1002 and by the U.S. DOE's Office of Energy Efficiency and Renewable Energy (EERE) under Solar Energy Technologies Office (SETO) Agreement DE-EE0008974. In addition, this work was authored in part by the National Renewable Energy Laboratory, operated by Alliance for Sustainable Energy, LLC, for the U.S. Department of Energy (DOE) under Contract No. DE-AC36-08GO28308. Funding provided U.S. Department of Energy Office of Energy Efficiency and Renewable Energy Solar Energy Technologies Office. The views expressed in the article do not necessarily represent the views of the DOE or the U.S. Government. The U.S. Government retains and the publisher, by accepting the article for publication, acknowledges that the U.S. Government retains a nonexclusive, paid-up, irrevocable, and worldwide license to publish or reproduce the published form of this work, or allow others to do so, for U.S. Government purposes. The authors thank Willard and Kelsey Solar Group for providing the CdS/CdTe samples.

■ REFERENCES

(1) Green, M. A.; Dunlop, E. D.; Hohl-Ebinger, J.; Yoshita, M.; Kopidakis, N.; Ho-Baillie, A. W. Y. Solar Cell Efficiency Tables (Version 55). *Prog. Photovoltaics* **2020**, *28*, 3−15.

(2) Gloeckler, M. In *Research Opportunities Supporting 25% CdTe PV*, MRS Spring Meeting, 2019.

(3) Barnard, E. S.; Ursprung, B.; Colegrove, E.; Moutinho, H. R.; Borys, N. J.; Hardin, B. E.; Peters, C. H.; Metzger, W. K.; Schuck, P. J. 3D Lifetime Tomography Reveals How CdCl2 Improves Recombination Throughout CdTe Solar Cells. *Adv. Mater.* **2017**, *29*, No. 1603801.

(4) Swanson, D. E.; Sites, J. R.; Sampath, W. S. Co-sublimation of CdSexTe1−x Layers for CdTe Solar Cells. *Sol. Energy Mater. Sol. Cells* **2017**, *159*, 389−394.

(5) Song, T.; Kanevce, A.; Sites, J. R. Emitter/absorber Interface of CdTe Solar Cells. *J. Appl. Phys.* **2016**, *119*, No. 233104.

(6) Kephart, J. M.; McCamy, J. W.; Ma, Z.; Ganjoo, A.; Alamgir, F. M.; Sampath, W. S. Band Alignment of Front Contact Layers for High-Efficiency CdTe Solar Cells. *Sol. Energy Mater. Sol. Cells* **2016**, *157*, 266−275.

(7) Kanevce, A.; Reese, M. O.; Barnes, T. M.; Jensen, S. A.; Metzger, W. K. The Roles of Carrier Concentration and Interface, Bulk, and Grain-boundary Recombination for 25% Efficient CdTe Solar Cells. *J. Appl. Phys.* **2017**, *121*, No. 214506.

(8) Duenow, J. N.; Metzger, W. K. Back-surface Recombination, Electron Reflectors, and Paths to 28% Efficiency for Thin-film Photovoltaics: A CdTe Case Study. *J. Appl. Phys.* **2019**, *125*, No. 053101.

(9) Liyanage, G. K.; Phillips, A. B.; Alfadhili, F. K.; Ellingson, R. J.; Heben, M. J. The Role of Back Buffer Layers and Absorber Properties for>25% Efficient CdTe Solar Cells. *ACS Appl. Energy Mater.* **2019**, *2*, 5419.

(10) Phillips, A. B.; Subedi, K. K.; Liyanage, G. K.; Alfadhili, F. K.; Ellingson, R. J.; Heben, M. J. Understanding and Advancing Bifacial Thin Film Solar Cells. *ACS Appl. Energy Mater.* **2020**, *3*, 6072.

(11) Bonilla, R. S.; Hoex, B.; Hamer, P.; Wilshaw, P. R. Dielectric Surface Passivation for Silicon Solar Cells: A Review. *Phys. Status Solidi* **2017**, *214*, No. 1700293.

(12) Schmidt, J.; Merkle, A.; Brendel, R.; Hoex, B.; de Sanden, M. V.; Kessels, W. M. M. Surface Passivation of High-efficiency Silicon Solar Cells by Atomic-layer-deposited Al2O3. *Prog. Photovoltaics* **2008**, *16*, 461−466.

(13) Jiang, Y.; Shen, H.; Yang, W.; Zheng, C.; Tang, Q.; Yao, H.; Raza, A.; Li, Y.; Huang, C. Passivation Properties of Alumina for Multicrystalline Silicon Nanostructure Prepared by Spin-coating Method. *Appl. Phys. A* **2018**, *124*, No. 95.

(14) Birant, G.; de Wild, J.; Meuris, M.; Poortmans, J.; Vermang, B. Dielectric-Based Rear Surface Passivation Approaches for Cu(In,Ga)-Se2 Solar Cells—A Review. *Appl. Sci.* **2019**, *9*, No. 677.

(15) Werner, F.; Veith-Wolf, B.; Melchiorre, M.; Babbe, F.; Schmidt, J.; Siebentritt, S. Ultra-thin passivation layers in Cu(In,Ga)Se2 thin-

film solar cells: full-area passivated front contacts and their impact on bulk doping. *Sci. Rep.* **2020**, *10*, No. 7530.
(16) Kephart, J. M.; Kindvall, A.; Williams, D.; Kuciauskas, D.; Dippo, P.; Munshi, A.; Sampath, W. S. Sputter-Deposited Oxides for Interface Passivation of CdTe Photovoltaics. *IEEE J. Photovoltaics* **2018**, *8*, 587−593.
(17) Kuciauskas, D.; Moseley, J.; Ščajev, P.; Albin, D. Radiative Efficiency and Charge-Carrier Lifetimes and Diffusion Length in Polycrystalline CdSeTe Heterostructures. *Phys. Status Solidi RRL* **2020**, *14*, No. 1900606.
(18) Werner, F.; Veith, B.; Tiba, V.; Poodt, P.; Roozeboom, F.; Brendel, R.; Schmidt, J. Very Low Surface Recombination Velocities on p- and n-type c-Si by Ultrafast Spatial Atomic Layer Deposition of Aluminum Oxide. *Appl. Phys. Lett.* **2010**, *97*, No. 162103.
(19) Meinander, K.; Preston, J. S. A DFT Study on the Effect of Surface Termination in CdTe (111)/α-Al2O3 (0001) Heteroepitaxy. *Surf. Sci.* **2015**, *632*, 93−97.
(20) Jovanovic, S. M.; Devenyi, G. A.; Jarvis, V. M.; Meinander, K.; Haapamaki, C. M.; Kuyanov, P.; Gerber, M.; LaPierre, R. R.; Preston, J. S. Optical Characterization of Epitaxial Single Crystal CdTe Thin Films on Al2O3 (0001) Substrates. *Thin Solid Films* **2014**, *570*, 155−158.
(21) Kuciauskas, D.; Kephart, J. M.; Moseley, J.; Metzger, W. K.; Sampath, W. S.; Dippo, P. Recombination Velocity Less than 100 cm/s at Polycrystalline Al2O3/CdSeTe Interfaces. *Appl. Phys. Lett.* **2018**, *112*, No. 263901.
(22) Liang, J.; Lin, Q.; Li, H.; Su, Y.; Yang, X.; Wu, Z.; Zheng, J.; Wang, X.; Lin, Y.; Pan, F. Rectification and Tunneling Effects Enabled by Al2O3 Atomic Layer Deposited on Back Contact of CdTe Solar Cells. *Appl. Phys. Lett.* **2015**, *107*, No. 013907.
(23) Werthen, J. G.; Häring, J. P.; Bube, R. H. Correlation Between Cadmium Telluride Surface Oxidation and Metal Junctions. *J. Appl. Phys.* **1983**, *54*, 1159−1161.
(24) Di, X.; Li, X.; Wang, D.; Li, Q.; Shen, K.; Wang, D. CdTe Thin Film Solar Cell with NiO as a Back Contact Buffer Layer. *Sol. Energy Mater. Sol. Cells* **2017**, *169*, 61−67.
(25) Watanabe, R.; Kawashima, M.; Saito, Y. Film Properties of Alumina Passivation Layer for Silicon Solar Cells Prepared by Spin-coating Method. *Thin Solid Films* **2015**, *590*, 98−102.
(26) Perkins, C. L.; McGott, D. L.; Reese, M. O.; Metzger, W. K. SnO2-Catalyzed Oxidation in High-Efficiency CdTe Solar Cells. *ACS Appl. Mater. Interfaces* **2019**, *11*, 13003−13010.
(27) Rugen-Hankey, S. L.; Clayton, A. J.; Barrioz, V.; Kartopu, G.; Irvine, S. J. C.; McGettrick, J. D.; Hammond, D. Improvement to Thin Film CdTe Solar Cells with Controlled Back Surface Oxidation. *Sol. Energy Mater. Sol. Cells* **2015**, *136*, 213−217.
(28) Perkins, C. L.; Ablekim, T.; Barnes, T. M.; Kuciauskas, D.; Nemeth, W.; Lynn, K. G.; Reese, M. O.; Swain, S. K.; Metzger, W. K. In *Interfaces Between CdTe and ALD Al2O3*, 7th World Conference on Photovoltaic Energy Conversion, 2018.
(29) Maruyama, T.; Arai, S. Aluminum Oxide Thin Films Prepared by Chemical Vapor Deposition from Aluminum Acetylacetonate. *Appl. Phys. Lett.* **1992**, *60*, 322−323.
(30) Pan, J.; Gloeckler, M.; Sites, J. R. Hole Current Impedance and Electron Current Enhancement by Back-contact Barriers in CdTe Thin Film Solar Cells. *J. Appl. Phys.* **2006**, *100*, No. 124505.
(31) Gessert, T. A.; Smith, S.; Moriatry, T.; Young, M.; Asher, S.; Johnston, S.; Duda, A.; DeHart, C.; Fahrenbruch, A. L. In *Evolution of CdS/CdTe Device Performance During Cu Diffusion*, Thirty-first IEEE Photovoltaic Specialists Conference, 2005; pp 291−294.

https://dx.doi.org/10.1021/acsami.0c12800
ACS Appl. Mater. Interfaces 2020, 12, 51337−51343